Article

Integrated Estimation Strategy of Brake Force Cooperated with Artificial Neural Network Based Road Condition Classifier and Vehicle Mass Identification Using Static Suspension Deflections

Nhat Nguyen Minh [1] and DaeYi Jung [2,*]

[1]   HUTECH Institute of Engineering, HUTECH University, Ho Chi Minh City 700000, Vietnam
[2]   Department of Mechanical and Automotive Engineering, Kunsan National University, Gunsan 54150, Korea
*   Correspondence: dyjung@kunsan.ac.kr

Abstract: Brake forces and maximum static road friction coefficients for each wheel of the vehicle are essential information for vehicle safety systems including adaptive cruise control, electronic stability control (ESC), and collision avoidance system, etc. Many studies have been performed to estimate brake force and road friction using well-known model-based approaches, but none have unambiguously guaranteed an accurate performance in all ranges of driving conditions and road ones. In addition, the investigation of the integrated estimation approach of road friction and brake force including mass estimation has not been clearly addressed so far. Therefore, in this study, a novel integrated estimation strategy based on a data-driven technique and artificial neural network (ANN) classifier along with a compact mass identification has been proposed to acquire the accurate road friction and brake force of individual wheel. Specifically, it includes an instant mass estimation by monitoring static suspension deflections, an artificial neural network (ANN) classifier for road friction coefficient based on the average data set from available standard sensors, and a brake force estimation using the data-driven technique. The performance of the proposed technique is validated by a co-simulation environment between Carsim and MATLAB/Simulink. It is found that the integrated estimation strategy guaranteed an accurate estimation of brake forces and road friction for a wide range of variations of road frictions, vehicle velocities, and masses. This work will be a valuable asset for those who wish to develop an integrated estimation system for such crucial parameters of the vehicle system.

Keywords: vehicle dynamics; estimation; brake force; road friction coefficient; vehicle mass estimation; integrated estimation system; artificial neural network (ANN) classifier; data-driven technique

1. Introduction

Active safety and intelligent control technologies in vehicles have been widely developed and applied, and most active safety systems will often benefit from a reliable and robust estimation of brake force. The brake force information is essential for a better tracking precision of potential trajectories, resulting in better vehicle control management. However, it is usually difficult to install sensors at contact points of the tires to collect the information directly due to the limited physical accessibility. Accordingly, it is more advantageous and beneficial for practical applications if we can develop methods to indirectly estimate or observe brake force based on the pre-existing sensor information.

In line with this sense, previous studies of indirect tire force estimation are actively conducted and can be classified into two major approaches. As the first stream, the tire model-based methods used analytical models such as Burckhardt static tire/road friction

model [1], Dugoff's model [2], and the most widely used, Pacejka model, also called "Magic formula" [3]. However, as all other static models, these models contain parameters that need to be estimated and disadvantages related to the inability to describe low slip effects. Meanwhile, as the second one, the sensor-based methods utilized EKF (Extended Kalman filtering) as a complex non-linear estimation technique to derive the tire force in [4]. Ref. [5] applied an EKBF (extended Kalman-Bucy filtering) and Bayesian hypothesis selection to estimate tire forces of vehicles on asphalt surfaces. An adaptive observer was constructed by combining a vehicle model and a tire force model by [6]. These approaches show accuracy and good robustness properties. Nonetheless, Refs. [4–6] generate inaccurate estimation results in some extreme road conditions and require a high computational complexity. Therefore, they are practically limited and often denied to be mounted in the commercial ECU (electronic control unit).

Fundamentally, according to Equation (1), to achieve a better result of tire force F_B during brake, we should identify the precise static maximum road friction coefficient μ_{max} and vertical tire forces F_z.

$$F_B = \mu_{max} F_z \tag{1}$$

Consequently, many various studies of tire-road friction modeling and estimation have been investigated. Holzmann [7] proposed a new predictive methodology for the estimation of μ by using a camera and a microphone. Sato [8] and Yamada [9] measured the wetness of the road by detecting reflected light using optical sensors. The disadvantages of these vision-based methods depend on the intensity and direction of light. Many commercial vehicles use a thermometer to warn drivers of icy roads. These cause-based methods detect the factors that change road friction. However, this method cannot reflect the vehicle driving conditions, such as variations in tire pressure, wear, or wheel dynamics. Moreover, the longitudinal dynamic based approaches are in general adopted for friction estimation. Many studies proposed friction coefficient identification strategies based on the concept "slip-slope" [10–13]. In all the approaches discussed above, the research results only focused on the estimation of the average tire-road friction coefficient for the entire vehicle.

On the other hand, the second element for brake force calculation is the vertical force at each tire as seen in Equation (1). These forces are determined by vehicle mass. Vahidi et al. [14,15] proposed an RLS (recursive least-square) mass and road grade estimation strategy that utilizes multiple forgetting factors to reflect a constant mass and time-varying road grade. RLS was also used in [16] and Ref. [17] combined with EKF to simultaneously estimate the electric bus mass and road grade. Meanwhile, Ref. [18] proposed a formulation to calculate the vehicle's mass essentially based on the knowledge of the vehicle's velocity and the engine torque, and Ref. [19] utilized engine torque local convex minimum characteristic to estimate the vehicle mass. The major problem in using these approaches is based on the fact that the vehicle is required to be driven to obtain the proper persistent excitation and it usually takes a considerable time to estimate the real mass value. Beatriz et al. [20] used information from suspension deflection sensors and a dual Kalman filter to estimate vehicle mass under static and dynamic conditions. Nowadays, vehicles equipped with active suspension incorporate these kinds of sensors. Suspension deflection can be directly measured through a potentiometer or an LVDT (linear variable differential transformer)) which are both relatively economical and practical to be used.

Taking into consideration all of the previous ideas and the fact that the studies of integrated brake force estimation system collaborated with road friction and vehicle mass estimators has not been sufficiently conducted, this paper proposes a novel longitudinal brake force estimation strategy for the individual wheel. Four major contributions clearly distinguish our endeavor from other studies:

Unlike [14–19], based on [20] but in a simpler way, the vehicle mass is instantly estimated by monitoring the static suspension deflections before the vehicle is driven by a driver or at a low speed of less than 10 km/h.

Road friction identification uses an artificial neural network and average data set from currently available standard sensors. Therefore, compared to the model-based and slip-slop approaches [7–13], the accuracy of estimation can be fortified because ANN directly learns the road condition from the actual data. Using the average data for ANN is also a distinguishable idea to obtain smooth estimation outcomes. In addition, due to the off-line training of ANN, the proposed classifier is computationally light thus it is possibly applicable to ECU for the actual road test and is engaged for individual wheel thus the identification of road conditions for each wheel is doable.

A combination of estimated mass, estimated road friction, and data-driven techniques is utilized to identify brake forces. The important aspect of this proposed brake force estimation structure relies on the estimation of the tire forces acting on each tire, without any reference to mathematical tire models [1–3]. Hence, compared to [4–6], it can be processed at a low computation cost, and a fast response, which makes the proposed method usable in middle-class cars with low-resolution sensors and low-performance microcontrollers.

This work provides us with another possible solution for the integrated estimation approach of road friction and brake force including mass estimation. As mentioned earlier, it is true that studies on such integrated estimation systems are insufficient.

Finally, the performance of the entire proposed estimation strategy is verified through several co-simulations between MATLAB/Simulink and a high-fidelity vehicle model from CarSim [21] according to different scenarios of velocities, road frictions, and masses.

The rest of this paper is organized as follows: Section 2 presents the problem formulation. Section 3 introduces longitudinal slip ratio and vertical load of each tire used in this paper. The main works, mass estimation, road friction estimation, and individual brake force estimation, are proposed in Sections 4–6, respectively. Details about the integrated estimation system are shown in Section 7. Simulation results are presented in Section 8, and Section 9 concludes this paper.

2. Problem Formulation

The overall integrated approach used in this paper for individual wheel brake force estimation consists of the following three steps:

(i) Vehicle mass estimation.

(ii) Road friction identification of each wheel (front-left (FL), front-right (FR), rear-left (RL), and rear-right (RR)) using an artificial neural network (ANN) classifier.

(iii) Individual wheel brake force estimation via a data-driven approach collaborated with estimated mass and road condition.

For a clear understanding of the proposed integrated system, the structure of the entire estimation system is described in Figure 1.

In the first step, the vehicle mass is estimated based on suspension deflections under the particular condition of vehicle velocity. A set of measurements for vehicle status is processed and then fed to a trained neural network for road friction estimation in the second step. Finally, the estimated values are taken as the known parameters in the third step to estimate the brake forces.

As the proposed estimator relies on longitudinal dynamics, similar to other model-based methods, the following pre-conditions for the activation of estimation are established:

(i) The estimation is activated when the brake is applied.

(ii) The steering wheel angle does not exceed 20 degrees.

(iii) The acceleration, yaw rate, longitudinal velocity, wheel speed, steering angle, brake pedal, and suspension deflection are assumed to be available during the estimation period.

When any of the above conditions are not satisfied, the estimation becomes inactive until all conditions are met again.
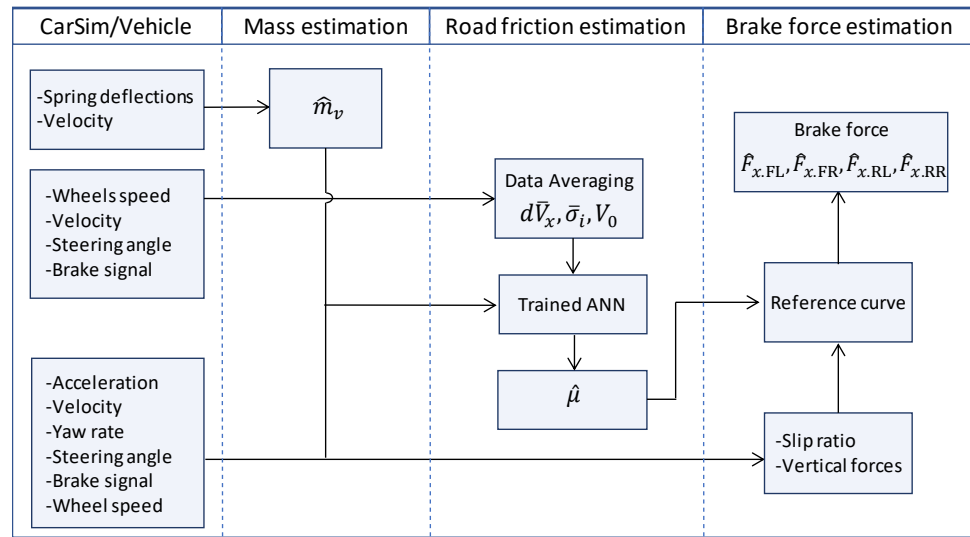
Figure 1. Entire structure of the proposed estimation systems.

3. Longitudinal Slip Ratio and Vertical Load of Each Wheel

Figure 2 presents the schematic diagram of the three-degrees-of-freedom (3-DoF) vehicle model used to compute the longitudinal slip ratio and vertical load of each wheel on the ground. The notation "CG" is the center of gravity (COG) of the whole vehicle. The value h_c is the height of COG relative to the ground and the distances from the vehicle's COG to the front and rear axles are l_f and l_r, respectively. The parameters t_f and t_r indicate the widths of front and rear track. The heading angle of the front tires are generated by the front steering wheel angle, δ. The side slip angle at the vehicle's COG is β described as the angle between the velocity vector V_c and the longitudinal velocity of the vehicle V_x. Moreover, $\dot{\psi}$ is the yaw rate of the vehicle. The lateral velocity of the vehicle is V_y. Furthermore, $F_{x,i}$ and $F_{y,i}$ represent the longitudinal and lateral forces acting on each tire, where sub-notations i indicate the front-left (FL), the front-right (FR), the rear-left (RL), and the rear-right (RR) tires of the vehicle. In addition, $F_{z,i}$ are the vertical forces of tires.
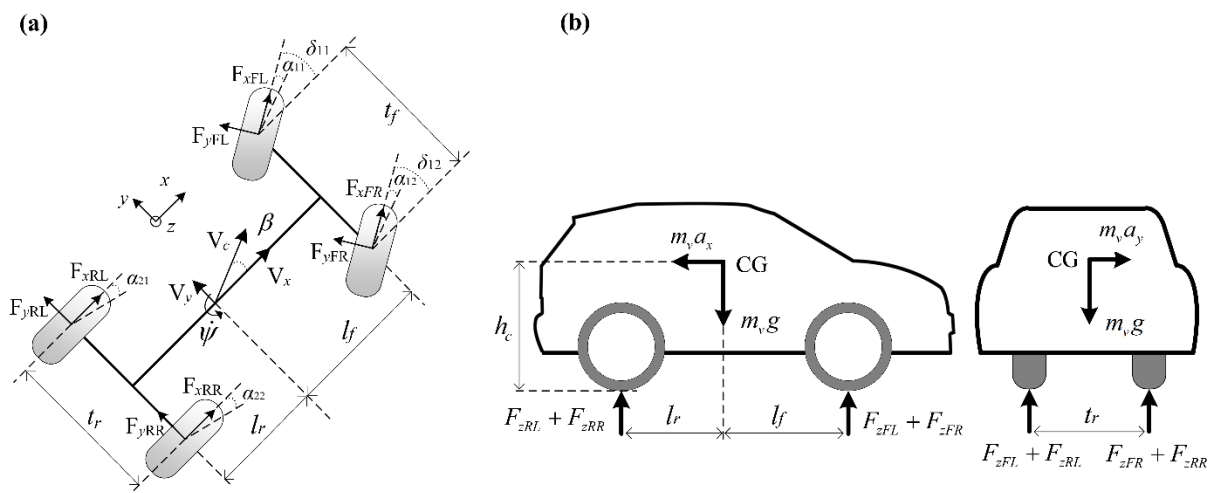
(a)   **(b)**

Figure 2. Schematic of 3-DOF vehicle model. (**a**) Vehicle planar model and (**b**) vehicle load transfer model.

Based on the difference between the actual longitudinal velocity at the wheel axle $V_{wx,i}$ and the equivalent rotational velocity $r_{eff}\omega_i$ of the tire, the longitudinal slip ratios can be defined as:

$$\sigma_i = \frac{r_{eff}\omega_i - V_{wx.i}}{\max\left(r_{eff}\omega_i, V_{wx.i}\right)} \quad i = FL, FR, RL, RR \tag{2}$$

where ω_i is the rotational speed of each wheel and r_{eff} is the effective radius of the tire.

Based on the vehicle's longitudinal (V_x), lateral velocity (V_y), and yaw rate ($\dot{\psi}$), the longitudinal velocity of each wheel $V_{wx.i}$ in (2) can be obtained [22]:

$$V_{wx.FL} = \left(V_x - \frac{\dot{\psi}\,t_f}{2}\right)\cos(\delta) + (V_x + \dot{\psi}\,l_f)\sin(\delta) \tag{3}$$

$$V_{wx.FR} = \left(V_x + \frac{\dot{\psi}\,t_f}{2}\right)\cos(\delta) + (V_x + \dot{\psi}\,l_f)\sin(\delta) \tag{4}$$

$$V_{wx.RL} = \left(V_x - \frac{\dot{\psi}\,t_r}{2}\right) \tag{5}$$

$$V_{wx.RR} = \left(V_x + \frac{\dot{\psi}\,t_r}{2}\right) \tag{6}$$

Considering the longitudinal and lateral acceleration of the vehicle, a_x and a_y, the vertical load of each wheel $F_{z,i}$ can be calculated as follows:

$$F_{z.FL} = m_v\left[g\frac{l_r}{2l} - a_x\frac{h_c}{2l} - a_y\frac{h_cl_r}{t_rl}\right] \tag{7}$$

$$F_{z.FR} = m_v\left[g\frac{l_r}{2l} - a_x\frac{h_c}{2l} + a_y\frac{h_cl_r}{t_rl}\right] \tag{8}$$

$$F_{z.RL} = m_v\left[g\frac{l_f}{2l} + a_x\frac{h_c}{2l} - a_y\frac{h_cl_f}{t_fl}\right] \tag{9}$$

$$F_{z.RR} = m_v\left[g\frac{l_f}{2l} + a_x\frac{h_c}{2l} + a_y\frac{h_cl_f}{t_fl}\right] \tag{10}$$

where, m_v is the total vehicle mass and g is the gravity acceleration constant. Moreover, $l = l_f + l_r$ is the wheelbase. All calculations presented here will be used for road friction and brake force estimations.

4. Vehicle Mass Estimation

The vehicle mass is one of the critical parameters for obtaining accurate vertical tire forces and road friction condition. Although many studies of mass estimation are carried out based on model-based approaches along with adaptive filters [14–19], they owned the limitation that the vehicle is required to be driven to obtain the proper persistent excitation and it requires a considerable estimation time. Therefore, this paper utilizes another method to estimate the vehicle mass based on the static load distribution by monitoring the static suspension deflections of all wheels [23] for quicker and more accurate results. Suspension deflection is assumed to be directly measured through a potentiometer or an LVDT (linear variable differential transformer) which are both economical and practical to be used. The advantage of this method is that it can be performed when the vehicle is stopped or is subject to a low speed thus it does not need to wait until the vehicle is subject to proper acceleration including persistent excitation. Moreover, the loading and unloading onto a vehicle are conducted when the vehicle is stopped. According to the loading condition, the suspension deflection is also changed. This variation can provide us with the increase or decrease of mass over the entire loading and unloading process.

The total mass of the vehicle is the sum of sprung mass m_s and un-sprung mass m_u. The un-sprung mass is seldom adjusted during vehicle operations. Hence, m_u is considered as a known constant in (11)

$$\widehat{m}_v = m_s + m_u \tag{11}$$

The variation in vehicle mass means the change of sprung mass due to the loading and unloading of either items or passengers (or both). Nevertheless, the sprung mass of the empty vehicle m_{s0} is given by the manufacturer. Thus,

$$m_s = m_{s0} + \Delta m_s \tag{12}$$

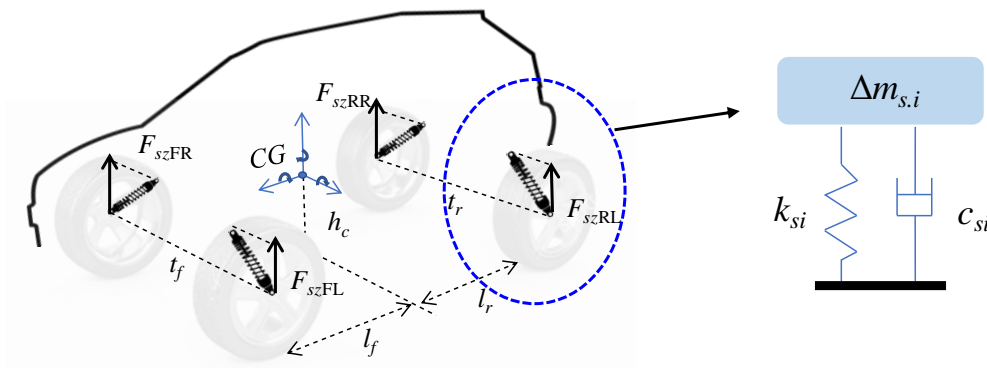In order to acquire the sprung mass variation, a quarter-car model in Figure 3 provides,

Figure 3. Spring forces acted on the wheel and quarter-car model.

$$\Delta m_s = \Delta m_{s.FL} + \Delta m_{s.FR} + \Delta m_{s.RL} + \Delta m_{s.RR} \tag{13}$$

The suspension springs are varied by the corresponding sprung mass on each side. Given a conventional suspension without level regulation, and assuming that it is operating within its linear range, an individual variation sprung mass, $\Delta m_{s.i}$, is defined,

$$\Delta m_{s.i} = \frac{F_{sz.i}}{g} = \frac{k_{si} \Delta s_i e_i}{g} \ for \ i = FL, FR, RL, RR \tag{14}$$

Here, Δs_i is the spring deflection variation from the initial deflection of the empty vehicle, k_i is the spring stiffness of the suspension, and e_i is the coefficient of spring force projection to the vertical axis.

Since this approach is valid in "stop" or "low speed" conditions with a less lateral motion of the vehicle, we set that the mass estimation is triggered at the conditions $V_x \leq$ 10 km/h and $SWA \leq 20^o$. The pseudo-code for the mass estimation is shown in the Algorithm 1.

Algorithm 1 Mass Estimation

Input $s_i, \ s_0, \ V_x, \ m_u, \ m_{s0}, \ k_i, \ g, \ e_i$

Output $\widehat{m}_{v.k}$

1: **If** $V_x < 10$km/h and $SWA \leq 20^o$ %SWA: Steering_Wheel_Angle

2:       $m_i = k_i e_i (s_i - s_0)/g$

3:       $\widehat{m}_v = \text{sum}(m_i) + m_u + m_{s0}$

4:       $\widehat{m}_{v.k} = \alpha \, \widehat{m}_{v.k-1} + (1-\alpha)\widehat{m}_v$ % Low-pass filter to obtain the smooth value

5:       $\widehat{m}_{v.k-1} = \widehat{m}_{v.k}$

6: **End**

---

5. Road Friction Estimation

As commonly known, it is not easy to obtain an accurate estimation of road friction for the various driving and road conditions based on the model-based approach inherently possessing the accumulated errors between the dynamic models. Thus, such model-based methods often lead to unexpected wrong consequences. Meanwhile, artificial neural networks have been increasingly applied to many engineering problems as they are able of capturing the complicated relations between inputs and outputs with a high approximation capacity. Therefore, in this study, we are willing to identify this complicated nonlinear relationship between the initial velocity at braking, average vehicle deceleration, estimated mass, average wheel slip ratio, and road friction using the ANN approach rather than the model-based approaches. The design of the proposed methodology is divided into two distinctive phases. In the first phase, data obtained from a set of sensors during brake are pre-processed before using as input data. In the second phase, an ANN model shown in Figure 4 is designed and includes the input layer (four nodes), three hidden layers (containing respectively twenty-five nodes, twenty-five nodes, and five nodes), as well as the output layer (one node). Moreover, each wheel is equipped with its own trained ANN classifier thus we can identify the individual frictions between road and wheels (i.e., FL, FR, RL, and RR) during the period of a brake.
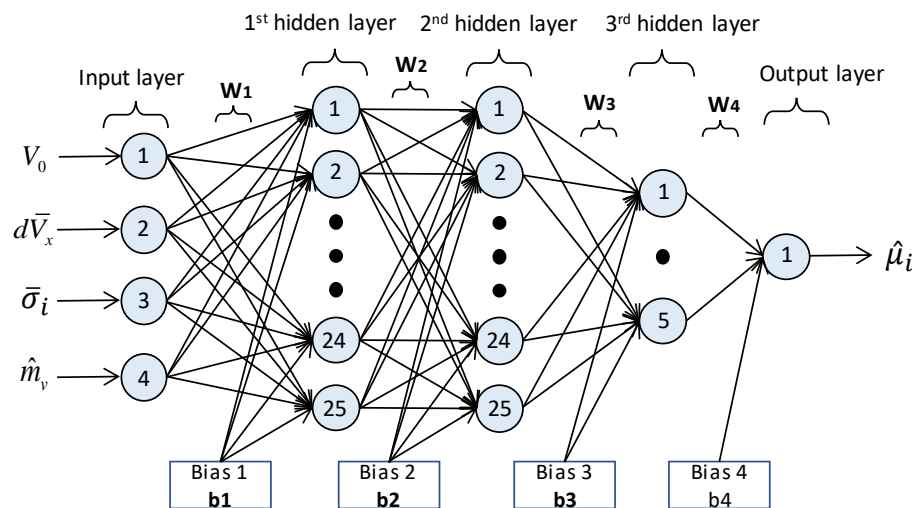

Figure 4. Proposed ANN structure (four inputs, three hidden layers, and one output).

5.1. Pre-Processing of Input Data

To achieve the proposed estimation strategy, the input vector of ANN is specifically chosen and described by $\mathbf{x} = [V_0 \; d\bar{V}_x \; \bar{\sigma}_i \; \hat{m}_v]^T \in \mathfrak{R}^{4 \times 1}$, which are, V_0 is the initial velocity at the braking moment, $d\bar{V}_x$ is the average velocity derivative (deceleration) of vehicle, $\bar{\sigma}_i$ (for i = FL, FR, RL, RR) is the average slip ratio of each wheel, and $\hat{m}_v$ is the estimated mass. These average values, $d\bar{V}_x$ and $\bar{\sigma}_i$, are calculated every twenty intervals. In other words, the average data are obtained every 0.02 s if the sampling time of the time-domain simulation process is set by 0.001 s. These "twenty" intervals are selected from the try-and-error method to achieve the best and reasonably quick estimation performance for other associated control systems.

The average velocity derivative $d\bar{V}_x$, one of the input data, is computed by,

$$d\bar{V}_x = \begin{cases} \frac{1}{N}\sum_{t=1}^{N}(V_{x.t} - V_{x.t-1})/\Delta t, \; 1 \text{ km/h} < V_x < 0.97 \, V_0 \\ \qquad\qquad d\bar{V}_x \,, V_x < 1 \text{ km/h} \end{cases} \tag{15}$$

where N = 20 intervals and V_0 is the vehicle velocity at the moment of braking. In addition, Δt indicates the sampling time.

The average slip ratio of each wheel $\bar{\sigma}_i$ (for i = FL, FR, RL, RR) are also calculated by,

$$\bar{\sigma}_i = \begin{cases} \frac{1}{N}\sum_{t=1}^{N}(\sigma_{i_t} - \sigma_{i_{t-1}}), 1 \text{ km/h} < V_x < 0.97\, V_0 \\ \bar{\sigma}_i, V_x < 1 \text{ km/h} \end{cases} \tag{16}$$

Again, it should be remarked that the average values, (15) and (16), are updated every twenty intervals, which implies that the road friction coefficient is updated every twenty intervals over the entire process.

5.2. Structure of ANN Classifier and Weight Tuning Algorithm

The total signals in the forward pass can be calculated as the following equations

$$\mathbf{a}_1 = f_1(\mathbf{W_1}\mathbf{x} + \mathbf{b_1}) \in \Re^{n \times 1} \tag{17}$$

$$\mathbf{a}_2 = f_2(\mathbf{W_2}\mathbf{a}_1 + \mathbf{b_2}) \in \Re^{n \times 1} \tag{18}$$

$$\mathbf{a}_3 = f_3(\mathbf{W_3}\mathbf{a}_2 + \mathbf{b_3}) \in \Re^{m \times 1} \tag{19}$$

$$\hat{\mu} = f_4(\mathbf{W_4}\mathbf{a_3} + b_4) \in \Re \tag{20}$$

where $\mathbf{x} \in \Re^{4 \times 1}$ is the input of the proposed ANN classifier. In addition, $\mathbf{W_1} \in \Re^{n \times 4}$, $\mathbf{W_2} \in \Re^{n \times n}$, $\mathbf{W_3} \in \Re^{m \times n}$, and $\mathbf{W_4} \in \Re^{1 \times m}$ (n = 25, m = 5) are the weight matrixes (or vectors) of the first hidden layer, the second hidden layer, the third hidden layer, and the output layer, respectively. $\mathbf{b_1} \in \Re^{n \times 1}$, $\mathbf{b_2} \in \Re^{n \times 1}$, $\mathbf{b_3} \in \Re^{m \times 1}$, $b_4 \in \Re$ are the bias vectors of the three hidden layers and the output layer. The activation function of the first hidden layer is the *tanh* function, and the *sigmoid* function is chosen as the activation function of the other layers and are given by,

$$f_1(*) = \frac{2}{(1 + \exp(-2*))} - 1 \tag{21}$$

$$f_i(*) = \frac{1}{(1 + \exp(-*))} \text{ for } i = 2,3,4 \tag{22}$$

where * indicates the input of the above functions. This proposed ANN employs a back-propagation algorithm [24] as the learning rule of a multi-layer neural network to find the optimal weights that can achieve the best mapping between inputs and output. Each weight and bias in (17) through (20) are updated in each iteration (specified as step k) based on the following rules,

$$\mathbf{W}_{i|k+1} = \mathbf{W}_{i|k} - \eta_W\left(\frac{\partial J}{\partial \mathbf{W}_{i|k}}\right) \text{ for } i = 1,2,3,4 \tag{23}$$

$$\mathbf{b}_{i|k+1} = \mathbf{b}_{i|k} - \eta_b\left(\frac{\partial J}{\partial \mathbf{b}_{i|k}}\right) \text{ for } i = 1,2,3,4 \tag{24}$$

where, η_W, η_b are the learning rates of weights and biases. The cross-entropy function is much more sensitive to the error [25]. Due to this reason, the learning rules derived from the cross-entropy function are generally known to yield better performance. The loss function J used here is defined as,

$$J = \sum_{s=1}^{M}[-\mathrm{e}_s \ln(\mathrm{e}_s) - (1 - \mathrm{e}_s)\ln(1 - \mathrm{e}_s)] \tag{25}$$

where M is the total number of training data and the error, $\mathrm{e}_s = \hat{\mu}_s - \mu$, between the outputs of ANN and true references. The specific updated laws are given in the Appendix A.

In addition, it should be noted that the training process will be conducted in the LAB environment (off-line procedure) and the best-fitted weights of ANN between input and output data will be transferred to the estimation algorithm for a validation process (furthermore to the controller (ECU) for the actual test). The flow diagram for the training and validation phases are briefly described in Figure 5.
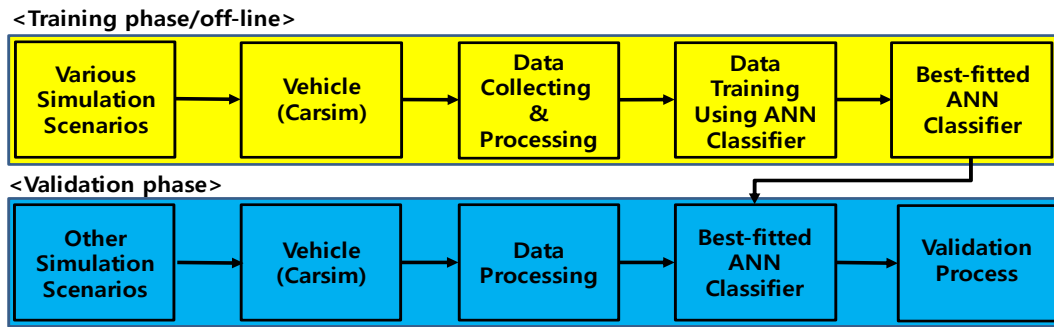
Figure 5. Training and validation phases.

The pseudo-codes of both data-processing and best-fitted ANN classifier in road friction estimation are shown in the Algorithm 2 and applied to the individual wheel.

Algorithm 2 Road Friction Estimation for Each Wheel

 # Data averaging process

Input ω_i, r_{eff}, V_x, $brake$, SWA, Δt %brake: Brake_Status/ SWA: Steering_Wheel_Angle

Output out_{V_o}, $\text{out}\_\bar{\sigma}_x$, $\text{out}\_d\bar{V}_x$

Initialization: flag $= 0$, $V_o = 0$, $\bar{\sigma}_i = 0$, $d\bar{V}_x = 0$, $\text{out}_{V_o} = 0$, $\text{out}_{d\bar{V}_x} = 0$,
$\qquad\qquad\qquad\quad \text{out}\_\bar{\sigma}_{xi} = 0$, count $= 0$, $\text{pre}\_V_x = 0$, $sum\_dV = 0$, $\text{sum}\_\sigma_i = 0$

1: **If** $brake > 0$ & flag $= 0$ & $SWA \leq 20^o$ %Condition to obtain V_0 at braking moment
2: $\qquad V_0 = V_x$
3: $\qquad$ flag $= 1$
4: **End**
5: **If** $brake > 0$ & flag $= 1$ & $SWA \leq 20^o$ %Estimation Condition
6: $\qquad$ **If** $V_x < 0.97 V_0$
7: $\qquad\qquad$ count $=$ count $+ 1$
8: $\qquad\qquad dV = (V_x - \text{pre}\_V_x)/\Delta t$
9: $\qquad\qquad$ sum$\_dV =$ sum$\_dV + dV$
10: $\qquad\qquad d\bar{V}_x =$ sum$\_dV$/count %Average Deceleration
11: $\qquad\qquad \sigma_i = (r_{eff}\omega_i - V_x)/\max(r_{eff}\omega_i, V_x)$
12: $\qquad\qquad$ sum$\_\sigma_i =$ sum$\_\sigma_i + \sigma_i$
13: $\qquad\qquad \bar{\sigma}_i =$ sum$\_\sigma_i$/count %Average slip ratio
14: $\qquad\qquad\qquad$ **If** count $= 20$ & $V_x > 5$ km/h %Reset Estimation Condition for next interval
15: $\qquad\qquad\qquad\qquad$ out$\_\sigma_i = \bar{\sigma}_i$
16: $\qquad\qquad\qquad\qquad$ out$\_d\bar{V}_x = d\bar{V}_x$
17: $\qquad\qquad\qquad\qquad$ out$\_V_0 = V_0$
18: $\qquad\qquad\qquad\qquad$ flag $= 0$
19: $\qquad\qquad\qquad\qquad$ count $= 0$
20: $\qquad\qquad\qquad\qquad$ sum$\_\sigma_i = 0$
21: $\qquad\qquad\qquad\qquad$ sum$\_dV = 0$
22: $\qquad\qquad\qquad$ **End**
23: $\qquad$ **End**
24: **End**
25: pre$\_V_x = V_x$ $\qquad$ %Replace the previous Vx with the current one

 # ANN classifier for individual wheel

Input out$\_V_o$, out$\_d\bar{V}_x$, out$\_\bar{\sigma}_i$, $\hat{m}_v$, W_{1i}, W_{2i}, W_{3i}, W_{4i}, b_{1i}, b_{2i}, b_{3i}, b_{4i}

Output $\hat{\mu}_i$

1: Data_in$_i = [\text{out}\_V_o/80$; out$\_d\bar{V}_x/10$; out$\_\bar{\sigma}_i$; $\hat{m}_v/4000]$ %Normalized
2: **If** out$\_d\bar{V}_x \neq 0$
3: $\quad a_1 = f_1(W_{1i}\text{Data\_in}_i + b_{1i})$
4: $\quad a_2 = f_2(W_{2i}a_1 + b_{2i})$
5: $\quad a_3 = f_3(W_{3i}a_2 + b_{3i})$
6: $\quad \hat{\mu}_i = f_4(W_{4i}a_3 + b_{4i})$
7: **Else**
8: $\quad \hat{\mu}_i = 0$
9: **End**

---

6. Individual Brake Force Estimation

In [1–6], it was pointed out that the brake force estimation has been performed by either sensor-based or model-based approaches. Unlike previous studies, we proposed the brake force estimation approach using a data-driven technique and CarSim tabular data combined with the estimated mass and estimated road friction to derive the individual brake force at each wheel. Thus, it is anticipated that the proposed method would be more cost-effective, accurate, and computationally efficient in practical application. In order to predict the rolling resistance, the shear forces and moments, and other related characteristics of the tire model, CarSim has built several nonlinear tables of the forces and moments [26], which are obtained by either measured in a laboratory or on-road tester as functions of vertical load, longitudinal slip, lateral slip, inclination angle, and tire/road friction. Figure 6 presents a 3D map that is constituted by reference curves representing the relationship between longitudinal forces and longitudinal slip ratios for nominal vertical load F_{z0} with $\mu_0 = 1$.
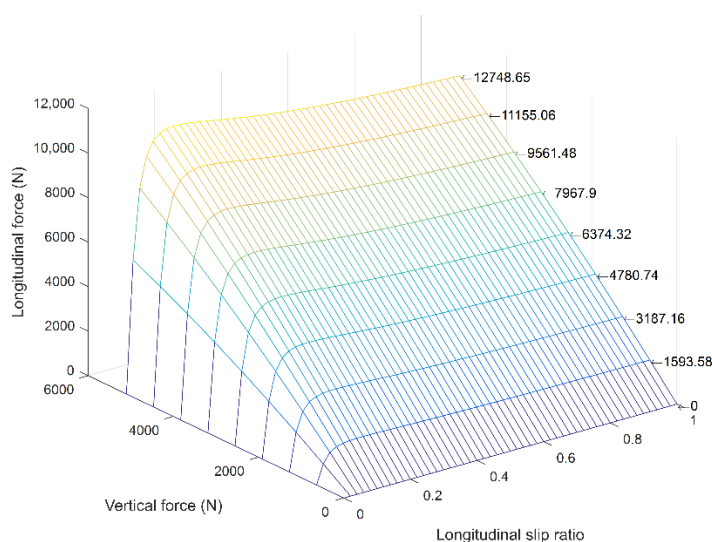
Figure 6. Three-dimensional map of longitudinal force corresponding to vertical force and slip ratio.

Furthermore, the tire behavior on different surfaces is obtained by a method so-called similarity in [27]. It predicts the change in limit shear force while maintaining the linear behavior for small amounts of change of slip ratio.

Thus, based on [27], the following equation for predicting the longitudinal force of each tire can be followed by,

$$F_{x.i} = \frac{\mu}{\mu_0} FX_0\left(F_{z.i}, \frac{\mu}{\mu_0}\sigma_i\right) \; for \; i = FL, FR, RL, RR \tag{26}$$

where μ is the current road friction coefficient.

FX_0 in (26) is extracted from the 3D map using linear interpolation and extrapolation techniques which indicates such a model function that represents the known data points, between or beyond the data range.

The procedure of the linear interpolation and extrapolation of FX_0 is as follows. Considering Figure 7, the estimated FX_0 is calculated by
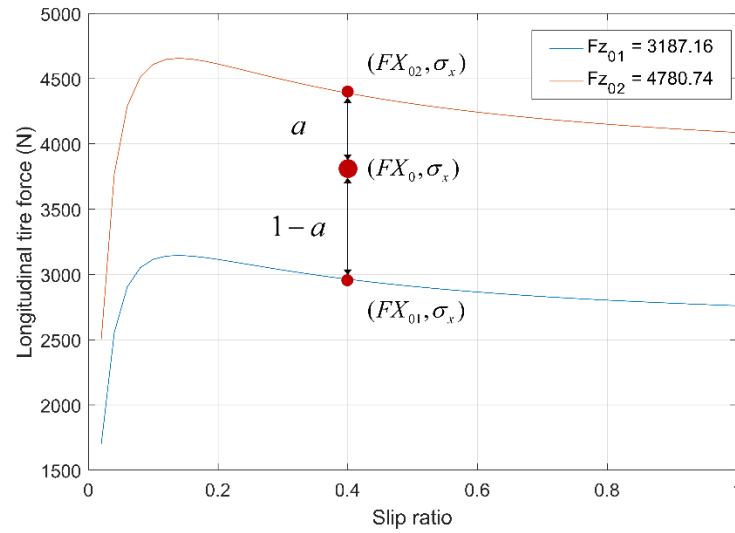
Figure 7. Reference curves of tire force in longitudinal direction.

$$FX_0 = (1-a)FX_{02} + aFX_{01} \tag{27}$$

Here, FX_{02} and σ_x are the longitudinal force and slip ratio of the reference curve measured at $Fz_{02} = 4780.74$ N. FX_{01} and σ_x are the longitudinal force and slip ratio of the reference curve measured at $Fz_{01} = 3187.16$ N. The parameter a is a constant for the interpolation, which has a relation with the vertical force and slip ratio as (28).

$$Fz_0 = (1-a)Fz_{02} + aFz_{01} \tag{28}$$

If $0 < a < 1$, the procedure is interpolation. If $a < 0$ or $a > 1$, the procedure is extrapolation. The pseudo-code for brake force estimation is shown in the Algorithm 3.

Algorithm 3 Brake Force Estimation

Input ω_i, r_{eff}, $V_{wx.i}$, μ_0, a_x, a_y, $\hat{\mu}_i$, $\hat{m}_v$, t_f, t_r, l_f, l_r, g, h

Output $\hat{F}_{x.\text{FL}}$, $\hat{F}_{x.\text{FR}}$, $\hat{F}_{x.\text{RL}}$, $\hat{F}_{x.\text{RR}}$

1: $\quad \sigma_{xi} = (r_{eff}\omega_i - V_{wx.i})/\max(r_{eff}\omega_i, V_{wx.i})$

2: $\quad F_{z.\text{FL}} = m_v \left[g\frac{l_r}{2l} - a_x\frac{h_c}{2l} - a_y\frac{h_c l_r}{t_r l} \right]$

3: $\quad F_{z.\text{FR}} = m_v \left[g\frac{l_r}{2l} - a_x\frac{h_c}{2l} + a_y\frac{h_c l_r}{t_r l} \right]$

4: $\quad F_{z.\text{RL}} = m_v \left[g\frac{l_f}{2l} + a_x\frac{h_c}{2l} - a_y\frac{h_c l_f}{t_f l} \right]$

5: $\quad F_{z.\text{RR}} = m_v \left[g\frac{l_f}{2l} + a_x\frac{h_c}{2l} + a_y\frac{h_c l_f}{t_f l} \right]$

6: $\quad p_i = \text{abs}(\sigma_{xi} * \mu_0/\hat{\mu}_i)$

7: $\quad p_i(p_i > 1.02) = 1.02$ %Set the upper limit of value

8: $\quad p_i(p_i < 0) = 0$ %Set the lower limit of value

9: **For i=1:1:4** % i=1 (FL)/ i=2 (FR)/ i=3 (RL)/ i=4 (RR),

10:$\hat{F}_{xi} = -\hat{\mu}_i/\mu_0 * (\text{interp2}(F_{x0}, F_{z0}, \sigma_0, F_{zi}, p_i, 'linear'))$

% The above F_{x0}, F_{z0} and σ_0 are reference values of 3D mapped longitudinal forces for the vertical force and slip ratio in Figure 6

11: **End**

---

7. Integrated Estimation System

When vehicle velocity is less than 10 km/h, the mass estimation is enabled to obtain and update the total vehicle mass. This mass value will be maintained at the specific value before the suspension of estimation if the estimation condition is not satisfied. The estimated total mass is used to calculate the individual vertical forces of tires via (7) through (10) for the brake force estimation. During vehicle operation, if the brake is applied and the steering wheel angle is smaller than 20 degs., the rest of the integrated estimation (road friction and brake force estimations) will be activated. Based on (15) and (16), the averaged input data of the trained ANN classifier are calculated by vehicle velocity and wheel speed. Then, based on the averaged data, the estimated road friction is produced by the ANN classifier. Finally, with the current estimates of road frictions on each wheel and estimated mass, the individual brake forces are identified by (26) together with (27) and (28).

8. Simulation Study

### 8.1. The Data Preparation and Training Phase

Here, we presented the training data set for the ANN classifier, which is coming from a co-simulation between CarSim and Simulink. A sedan C-class with four-wheel drive, specified in Table 1, is selected from CarSim. The data obtained from the co-simulations are the vehicle velocity, acceleration, wheel speed, brake control signal, and steering angle. Using an Algorithm 2 based on (15) and (16), the data shown in Figure 8 have been generated. The vehicle model with different masses of 1642 kg (Group1), 1842 kg (Group2), and 2042 kg (Group3) runs at three random target speeds, 25 km/h, 79 km/h, and 107 km/h and then the brake is applied until the vehicle is completely stopped. Each brake cycle is performed at different road friction ranging from 0.1~1. Hence, the training data set is constructed from ninety simulations. The label data (true references) for ANN training is presented in Figure 9. The ANN training strategy follows the diagram described in Figure 10 thus the training will be continued until the acceptable error between true references and estimates (outputs of trained ANN) is achieved. The ANN classification performance of each wheel is shown in Figure 11, where comparison results indicate well trained ANN for a wide range of data.

**Table 1.** Simulation vehicle configuration.

| Vehicle Model	Specification
Type	C-class
Brake	ABS at 4 wheels
Powertrain	150 kW, 6 speeds
Tires	215/55 R17
Suspension	Independent
Total mass of the empty vehicle	1642 kg
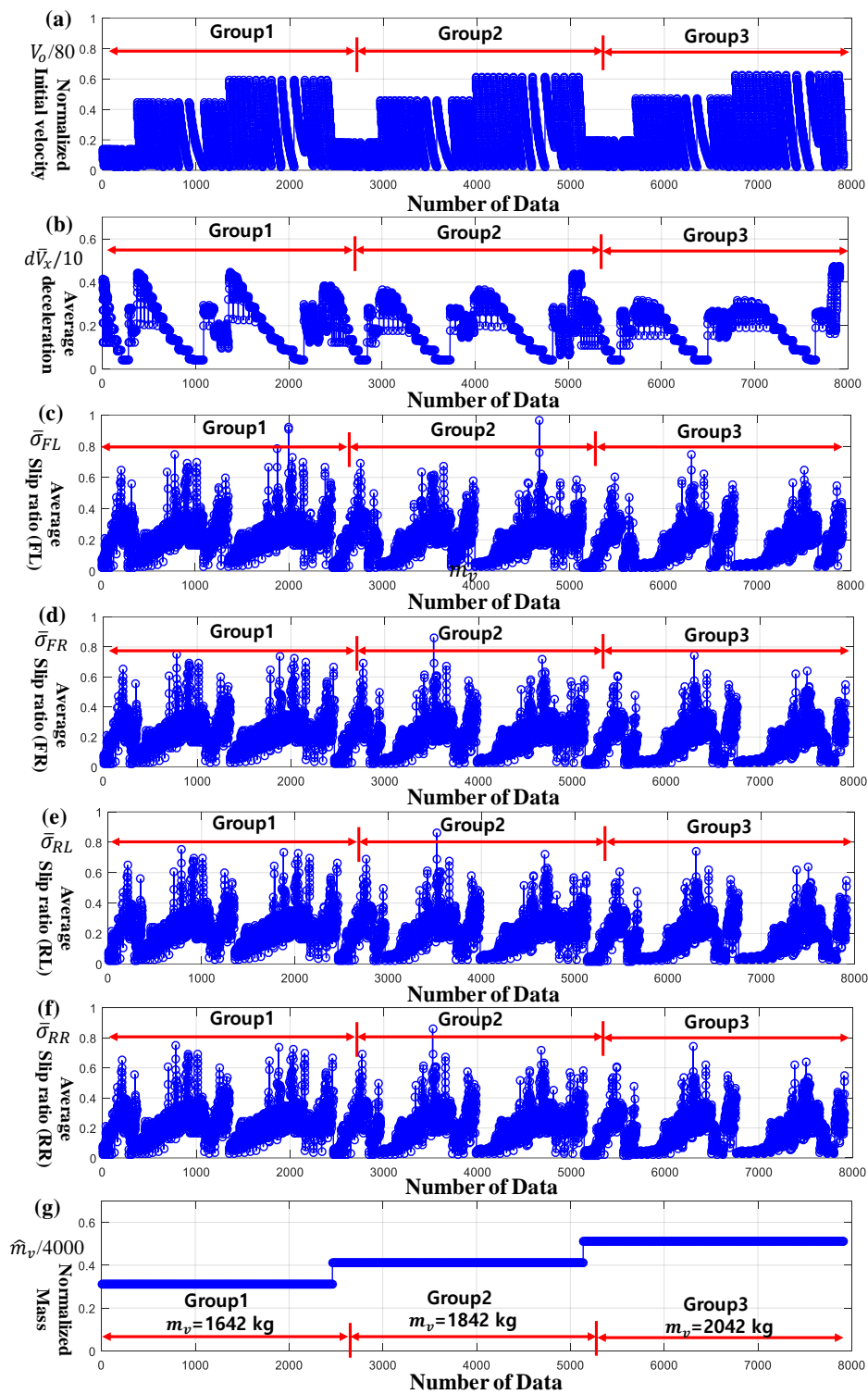
Figure 8. Input training data set (**a**) Normalized initial velocity at the braking (V_0), (**b**) normalized average deceleration (dV_{aver}), (**c**) average front-left wheel slip ratio (FL), (**d**) average front-right wheel slip ratio (FR), (**e**) average rear-left wheel slip ratio (RL), (**f**) average rear-right wheel slip ratio (RR), and (**g**) normalized vehicle mass.
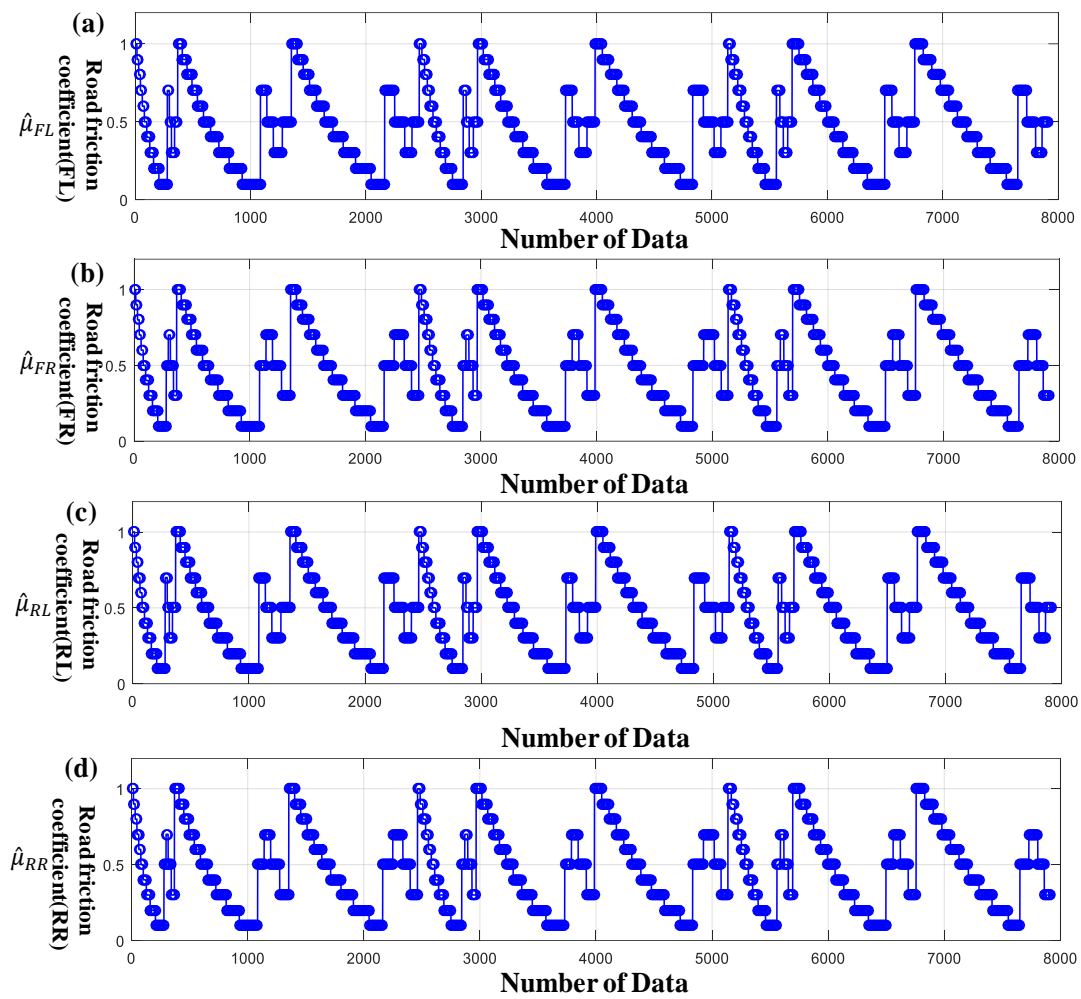
Figure 9. True references for training data (road friction coefficients). (**a**) Front left wheel (FL), (**b**) front right wheel (FR), (**c**) rear left wheel (RL), and (**d**) rear right wheel (RR).
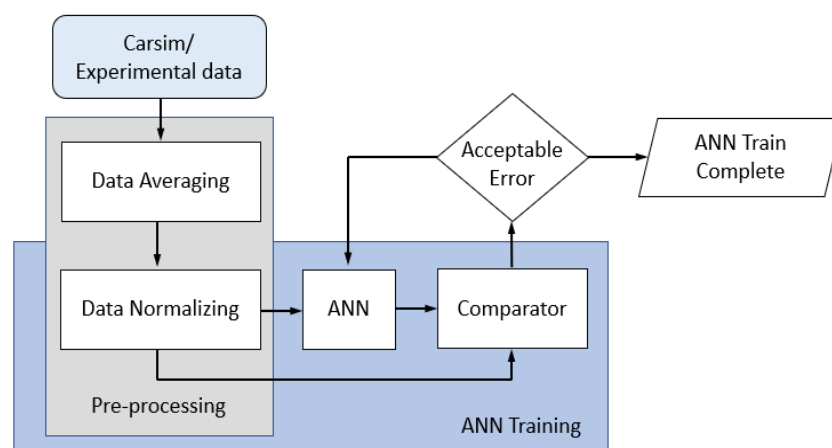

Figure 10. ANN training diagram.
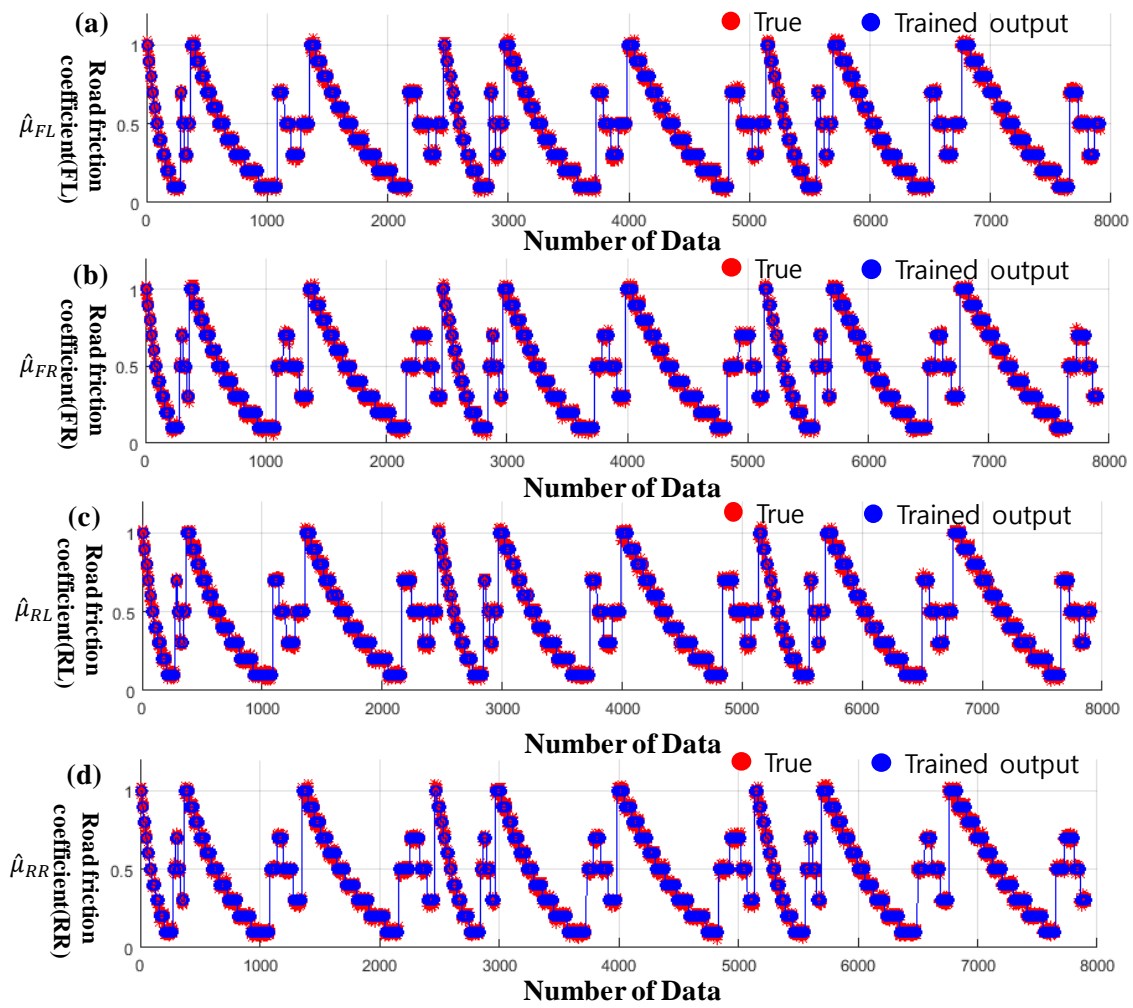
Figure 11. Comparison between true references and trained outputs. (**a**) Front left wheel, (FL) (**b**) front right wheel (FR), (**c**) rear left wheel (RL), and (**d**) rear right wheel (RR).

8.2. The Validation Phase

Figure 12 explores the effectiveness of the proposed mass estimation approach as described in Algorithm 1. In Figure 12, the performance of the system has been verified by three different masses m_v = 1780 kg, m_v = 1980 kg, and m_v = 2180 kg. Again, it should be noted that the estimation is disabled when the longitudinal velocity becomes greater than 10 km/h (i.e., V_x > 10 km/h). In addition, as shown in Figure 12b,e,h, the suspension springs are varied by the corresponding sprung mass when the vehicle is accelerated from 0 velocity. The estimated mass quickly converges to the true value almost less than 0.3 s, as shown in Figure 12c,f,i.
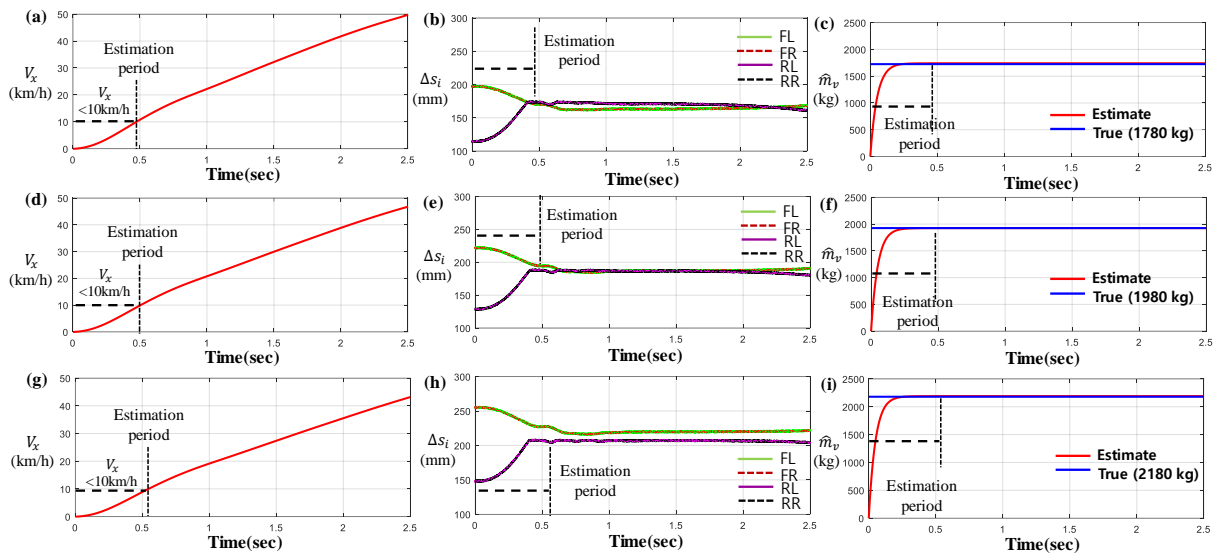
Figure 12. Mass estimation results. (**a**) Longitudinal velocity (1780 kg), (**b**) suspension deflections (1780 kg), (**c**) mass estimation (1780 kg), (**d**) longitudinal velocity (1980 kg), (**e**) suspension deflections (1980 kg), (**f**) mass estimation (1980 kg), (**g**) longitudinal velocity (2180 kg), (**h**) suspension deflections (2180 kg), and (**i**) mass estimation (2180 kg).

Here, we discussed the performance of the trained ANN classifier presented in Algorithm 2 and the incorporation of brake force estimation described in Algorithm 3. First, based on the scenario shown in Figure 13a, the loaded vehicle with mass m_v = 1800 kg has been accelerated to 100 km/h and then was braked ($P_m > 0$) at 10 secs until the vehicle completely stops. After the first stop, a second acceleration was initiated and proceeded to reach 60 km/h, and then a brake ($P_m > 0$) was again applied at 27 s. As shown in Figure 13b, the road frictions are assumed to be randomly changed during each brake.

Figure 13b indicates that the vehicle experiences four-times abrupt changes in friction level during the first brake and twice at the second brake. It can be seen that the estimated friction excellently tracks the abrupt changes of the true friction. Although there are small errors at 15 s, the overall results are acceptable.

Moreover, the brake forces estimated by the proposed method accurately track their true values as seen in Figure 13c–f. The most challenging change was the one occurred at 10 s, where the car takes a longer time to reach the trigger value ($V_x = 0.97V_0$) due to the low road friction ($\mu = 0.1$). Therefore, the convergence to the reference brake forces exhibits a small delay right after the first brake. Moreover, the friction estimation mainly affects the accuracy of the estimated brake force since estimation results are varied by the accuracy of road friction. From Figure 13d, we can see that the estimation error of the front-right wheel at 14 s is larger than others because the front-right friction ($\hat{\mu}_{FR}$) is underestimated (see Figure 13b).
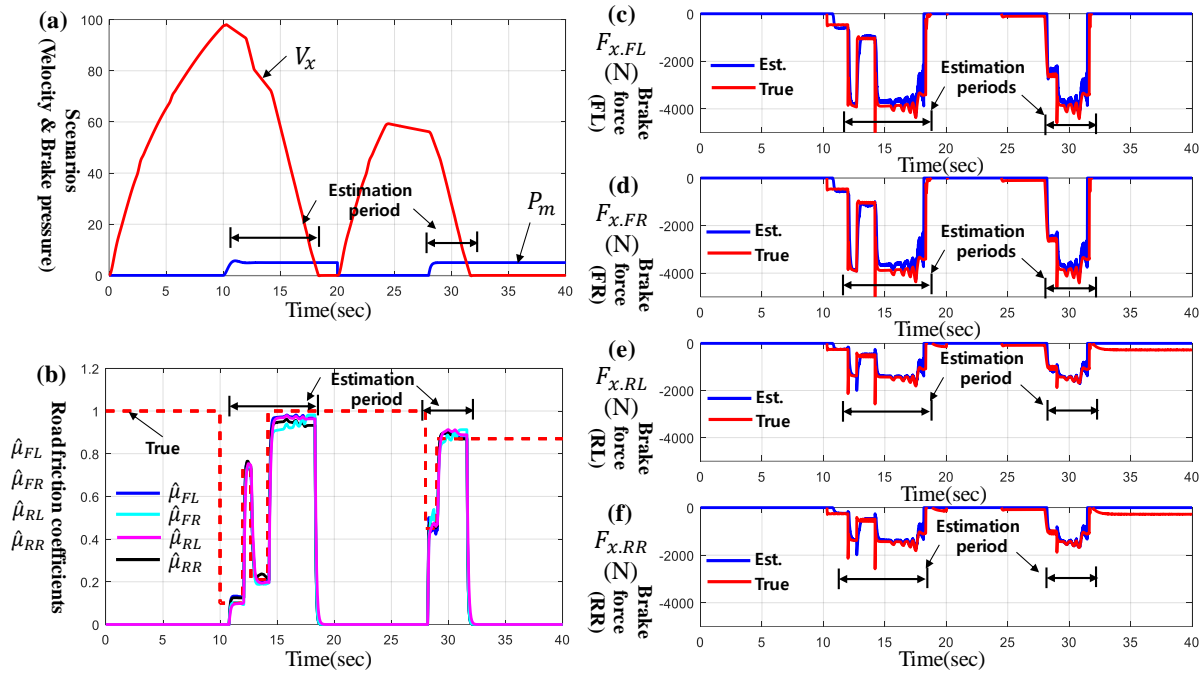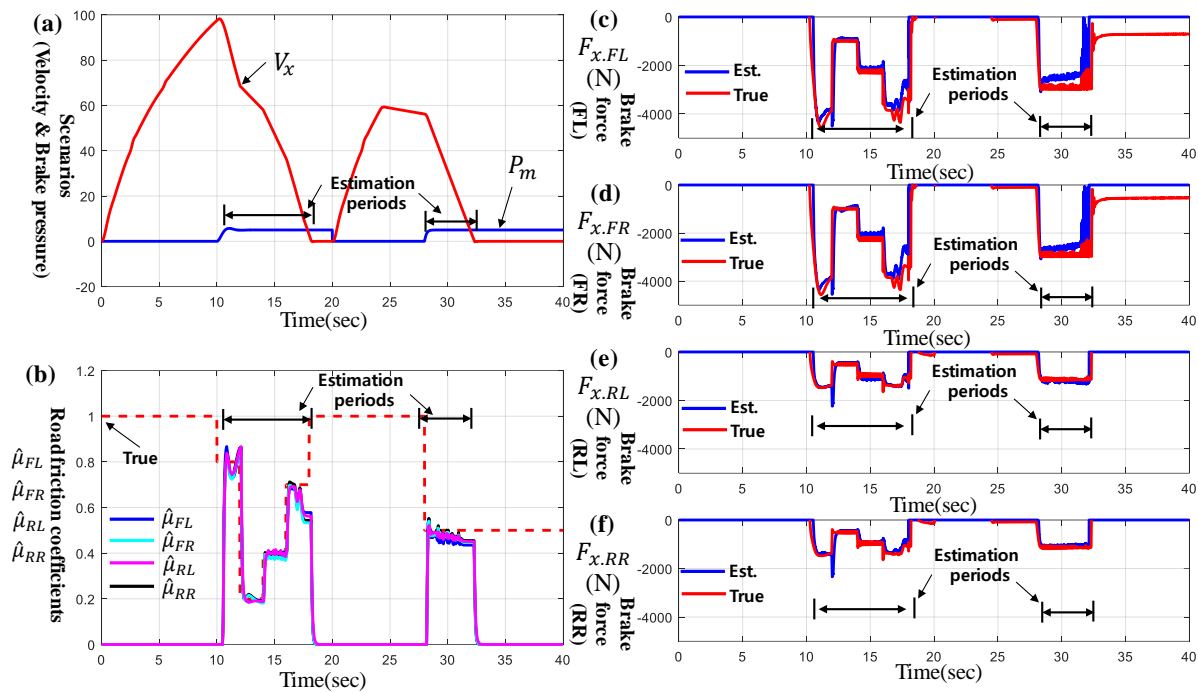
Figure 13. Estimation results of road friction coefficients and brake forces with m_v = 1800 kg. (**a**) Vehicle speed and brake scenarios, (**b**) estimates of road friction coefficients, (**c**) brake force of FL wheel, (**d**) brake force of FR wheel, (**e**) brake force of RL wheel, and (**f**) brake force of RR wheel.

The second test has been obtained from the same setup but with a different vehicle mass m_v = 2100 kg and other road friction patterns during two brake cycles. Again, the results shown in Figure 14b indicate that the individually estimated road friction adapts the actual value quickly and accurately. Figure 14c–f describes the estimation of the longitudinal braking forces. Nevertheless, there are momentarily differences between the true values and estimates when the friction level is abruptly changed. The main source of these discrepancies is the delay of averaging data process. The values of averaged slip ratio $\bar{\sigma}_i$ and averaged deceleration $d\bar{V}_x$ do not update to new values until satisfying *count* = 20 (see Algorithm 2). This can be observed clearly at the 12 s of the first brake.

Table 2 shows the correlation between actual brake force and the estimated one based on the following performance index, the correlation coefficient,

$$C = \frac{n(\sum xy) - (\sum x)(\sum y)}{\sqrt{[n(\sum x^2) - (\sum x)^2][n(\sum y^2) - (\sum y)^2]}} \tag{29}$$

where n is the sample size, x is the true value from CarSim of the concerned wheel, and y is the estimated value of the concerned wheel. According to the correlation coefficient in Table 2, the braking force coincides with the actual one by more than 87%, at least.
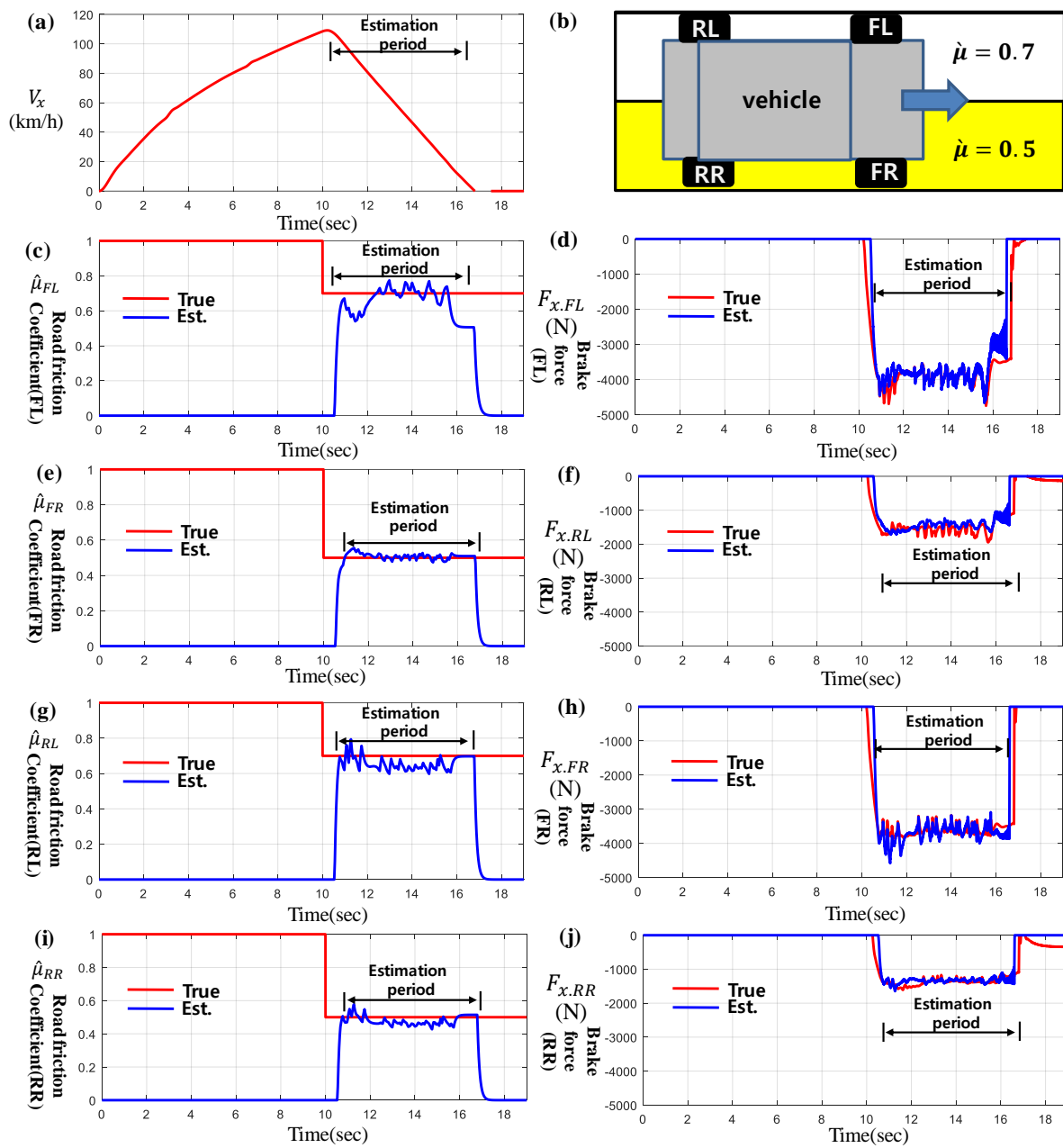
Figure 14. Estimation results of road friction coefficients and brake forces with m_v = 2100 kg. (**a**) Vehicle speed and brake scenarios, (**b**) estimates of road friction coefficients, (**c**) brake force of FL wheel, (**d**) brake force of FR wheel, (**e**) brake force of RL wheel, and (**f**) brake force of RR wheel.

Table 2. Correlation coefficient for data comparison of brake forces for Figures 13 and 14.

	Front Axle	**Rear Axle**
First brake (Figure 13)	Left: 92.93% match	Left: 90.08% match
	Right: 93.5% match	Right: 92.02% match
Second brake (Figure 14)	Left: 89.85% match	Left: 87.95% match
	Right: 88.60% match	Right: 87.09% match

Additional simulation results for a split-friction road surface, the different values of friction coefficients on the left- and right-hand sides of the vehicle, are presented in Figures 15 and 16. Full braking has been applied at around 10 s after the vehicle reaches 110 km/h. Figures 15c,e,g,i and 16c,e,g,i show that the reasonably accurate estimation of road friction for each wheel has been made. Moreover, the estimates of the corresponding four brake forces are well synchronous with the true values as seen in Figures 15d,f,h,j and 16d,f,h,j. Table 3 lists the correlation coefficient between true brake force and the estimated one showing the matching rate is at least more than 90%.

Figure 15. Estimation results of road friction coefficients and brake forces for split-friction road. (**a**) Longitudinal vehicle speed, (**b**) split-friction road condition ($\hat{\mu} = 0.7$ for left and $\hat{\mu} = 0.5$ for right), (**c**) friction estimation of FL wheel, (**d**) brake force of FL wheel, (**e**) friction estimation of FR wheel, (**f**) brake force of FR wheel, (**g**) friction estimation of RL wheel, (**h**) brake force of RL wheel, (**i**) friction estimation of RR wheel, and (**j**) brake force of RR wheel.
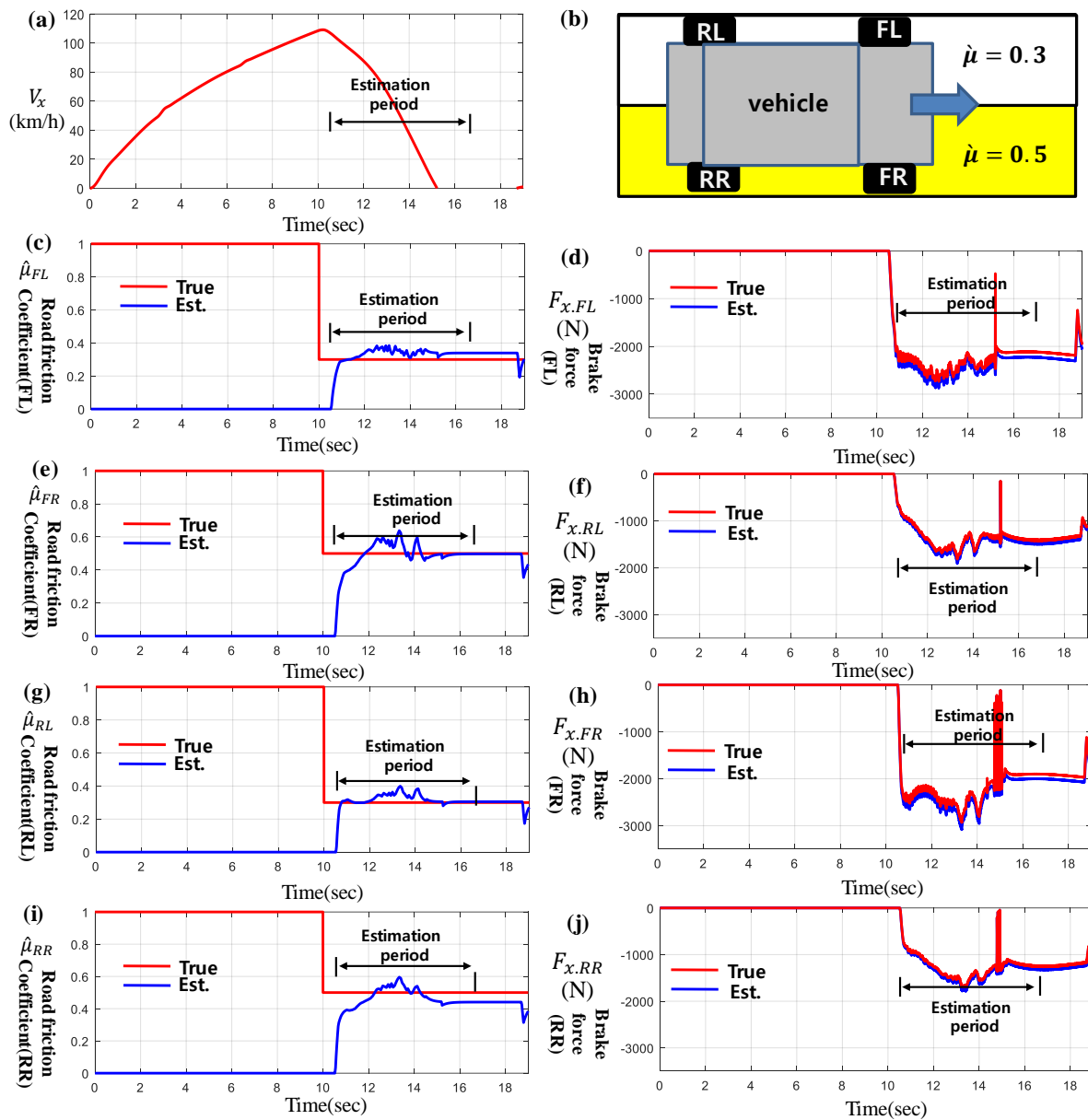
Figure 16. Estimation results of road friction coefficients and brake forces for split-friction road. (**a**) Longitudinal vehicle speed, (**b**) split-friction road condition ($\hat{\mu} = 0.3$ for left and $\hat{\mu} = 0.5$ for right), (**c**) friction estimation of FL wheel, (**d**) brake force of FL wheel, (**e**) friction estimation of FR wheel, (**f**) brake force of FR wheel, (**g**) friction estimation of RL wheel, (**h**) brake force of RL wheel, (**i**) friction estimation of RR wheel, and (**j**) brake force of RR wheel.

Table 3. Correlation coefficient for data comparison of brake forces for Figures 15 and 16.

	Front Axle	**Rear Axle**
First brake (Figure 15)	Left: 93.03% match	Left: 93.08% match
	Right: 96.21% match	Right: 92.12% match
Second brake (Figure 16)	Left: 90.85% match	Left: 91.05% match
	Right: 93.60% match	Right: 95.09% match

It is obvious from Figure 13 through Figure 16 that the proposed estimation approaches provide us with a fast and robust estimation of the brake force on either friction-transition road surface (Figures 13 and 14) or split-friction road surface (Figures 15 and 16) during the brake period.

The overall results exhibit reasonable and acceptable performance in various driving and road conditions, based only on the basic sensors already installed in vehicle stability control systems.

9. Conclusions

This paper presents a novel longitudinal brake force estimation strategy for individual wheels using an artificial neural network classifier and data-driven technique together.

(i) The vehicle mass was instantly estimated by monitoring the static suspension deflections.

(ii) Road friction identification used an artificial neural network and average data set from currently available standard sensors.

(iii) A combination of estimated mass, estimated road friction, and data-driven technique was utilized to estimate brake forces.

The proposed approach was verified through several co-simulation between CarSim and Matlab/Simulink with different velocities, road friction, and masses. In several braking cycles, the estimation performance of the brake force was satisfactory, the minimum correlation coefficient was 87% match between the estimated force and its actual value. It can be concluded that the proposed method can guarantee robustness for a wide range of road friction (including abrupt changes in road conditions) and mass variation.

The important aspect of this proposed brake force estimation structure relies on the estimation of the tire forces acting on each tire, without reference to any specific tire model. Hence, it can be processed at a low computation cost, a fast response. This work enables us to apply the proposed method in middle-class cars, for which low-resolution sensors and low-performance microcontrollers are used. Future studies will verify the proposed strategy by conducting actual vehicle tests.

Author Contributions: Formal analysis, N.N.M.; Writing—review & editing, D.J. All authors have read and agreed to the published version of the manuscript.

Conflicts of Interest: The authors declare no conflict of interest.

Appendix A

The updated law of W_4

$$\frac{\partial J}{\partial W_4} = \sum_{i=1}^{n} \frac{\partial J}{\partial a_4} \frac{\partial a_4}{\partial y_4} \frac{\partial y_4}{\partial W_4} = \sum_{i=1}^{n} \frac{a_4 - \mu}{a_4(1 - a_4)} a_4(1 - a_4)a_3 = \sum_{i=1}^{n} (a_4 - \mu)a_3$$

The updated law of b_4

$$\frac{\partial J}{\partial b_4} = \sum_{i=1}^{n} \frac{\partial J}{\partial a_4} \frac{\partial a_4}{\partial y_4} \frac{\partial y_4}{\partial b_4} = \sum_{i=1}^{n} \frac{a_4 - \mu}{a_4(1 - a_4)} a_4(1 - a_4) = \sum_{i=1}^{n} (a_4 - \mu)$$

The updated law of W_3

$$\frac{\partial J}{\partial W_3} = \sum_{i=1}^{n} \frac{\partial J}{\partial a_4} \frac{\partial a_4}{\partial y_4} \frac{\partial y_4}{\partial a_3} \frac{\partial a_3}{\partial y_3} \frac{\partial y_3}{\partial W_3} = \sum_{i=1}^{n} \frac{a_4 - \mu}{a_4(1 - a_4)} a_4(1 - a_4){W_4}^T a_3 (1 - a_3){a_2}^T = \sum_{i=1}^{n} (a_4 - \mu){W_4}^T a_3(1 - a_3){a_2}^T$$

The updated law of b_3

$$\frac{\partial J}{\partial b_3} = \sum_{i=1}^{n} \frac{\partial J}{\partial a_4} \frac{\partial a_4}{\partial y_4} \frac{\partial y_4}{\partial a_3} \frac{\partial a_3}{\partial y_3} \frac{\partial y_3}{\partial b_3} = \sum_{i=1}^{n} \frac{a_4 - \mu}{a_4(1-a_4)} a_4(1-a_4) W_4^T a_3 (1-a_3) = \sum_{i=1}^{n} (a_4 - \mu) W_4^T a_3(1-a_3) \tag{A1}$$

The updated law of W_2

$$\frac{\partial J}{\partial W_2} = \sum_{i=1}^{n} \frac{\partial J}{\partial a_4} \frac{\partial a_4}{\partial y_4} \frac{\partial y_4}{\partial a_3} \frac{\partial a_3}{\partial y_3} \frac{\partial y_3}{\partial a_2} \frac{\partial a_2}{\partial y_2} \frac{\partial y_2}{\partial W_2} = \sum_{i=1}^{n} \frac{a_4 - \mu}{a_4(1-a_4)} a_4(1-a_4) W_4^T a_3 (1-a_3) W_3^T a_2(1-a_2) a_1^T$$

$$= \sum_{i=1}^{n} (a_4 - \mu) W_4^T a_3(1-a_3) W_3^T a_2(1-a_2) a_1^T$$

The updated law of b_2

$$\frac{\partial J}{\partial b_2} = \sum_{i=1}^{n} \frac{\partial J}{\partial a_4} \frac{\partial a_4}{\partial y_4} \frac{\partial y_4}{\partial a_3} \frac{\partial a_3}{\partial y_3} \frac{\partial y_3}{\partial a_2} \frac{\partial a_2}{\partial y_2} \frac{\partial y_2}{\partial b_2} = \sum_{i=1}^{n} \frac{a_4 - \mu}{a_4(1-a_4)} a_4(1-a_4) W_4^T a_3 (1-a_3) W_3^T a_2(1-a_2)$$

$$= \sum_{i=1}^{n} (a_4 - \mu) W_4^T a_3(1-a_3) W_3^T a_2(1-a_2) \tag{A2}$$

The updated law of W_1

$$\frac{\partial J}{\partial W_1} = \sum_{i=1}^{n} \frac{\partial J}{\partial a_4} \frac{\partial a_4}{\partial y_4} \frac{\partial y_4}{\partial a_3} \frac{\partial a_3}{\partial y_3} \frac{\partial y_3}{\partial a_2} \frac{\partial a_2}{\partial y_2} \frac{\partial y_2}{\partial a_1} \frac{\partial a_1}{\partial y_1} \frac{\partial y_1}{\partial W_1}$$

$$= \sum_{i=1}^{n} \frac{a_4 - \mu}{a_4(1-a_4)} a_4(1-a_4) W_4^T a_3 (1-a_3) W_3^T a_2(1-a_2) W_2^T (1-a_1^2) x'$$

$$= \sum_{i=1}^{n} (a_4 - \mu) W_4^T a_3(1-a_3) W_3^T a_2(1-a_2) W_2^T (1-a_1^2) x'$$

The updated law of b_1

$$\frac{\partial J}{\partial b_1} = \sum_{i=1}^{n} \frac{\partial J}{\partial a_4} \frac{\partial a_4}{\partial y_4} \frac{\partial y_4}{\partial a_3} \frac{\partial a_3}{\partial y_3} \frac{\partial y_3}{\partial a_2} \frac{\partial a_2}{\partial y_2} \frac{\partial y_2}{\partial a_1} \frac{\partial a_1}{\partial y_1} \frac{\partial y_1}{\partial W_1}$$

$$= \sum_{i=1}^{n} \frac{a_4 - \mu}{a_4(1-a_4)} a_4(1-a_4) W_4^T a_3 (1-a_3) W_3^T a_2(1-a_2) W_2^T (1-a_1^2)$$

$$= \sum_{i=1}^{n} (a_4 - \mu) W_4^T a_3(1-a_3) W_3^T a_2(1-a_2) W_2^T (1-a_1^2)$$

References

1. Reimpell, M.B.J.R. *Fahrwerktechnik Radschlupf–Regelsysteme*; Vogel: Wrzburg, Germany, 1993.
2. Dugoff, H.; Fancher, P.S.; Segel, L. An Analysis of Tire Traction Properties and Their Influence on Vehicle Dynamic Performance. *SAE Trans.* **1970**, *79*, 1219–1243.
3. Bakker, E.; Pacejka, H.B.; Lidner, L. *A New Tire Model with an Application in Vehicle Dynamics Studies*; SAE Technical Paper 890087; SAE: Warrendale, PA, USA, 1989. https://doi.org/10.4271/890087.
4. Dakhlallah, J.; Glaser, S.; Mammar, S.; Sebsadji, Y. Tire-road Forces Estimation Using extended Kalman Filter and Sideslip Angle Evaluation. In Proceedings of the 2008 American Control Conference, Seattle, WA, USA, 11–13 June 2008; pp. 4597–4602.
5. Ray, L.R. Nonlinear Tire Force Estimation and Road Friction Identification: Simulation and Experiments. *Automatica* **1997**, *33*, 1819–1833.
6. Baffet, G.; Charara, A.; Dherbomez, G. An Observer of Tire–Road Forces and Friction for Active Security Vehicle Systems. *IEEE/ASME Trans. Mechatron.* **2007**, *12*, 651–661.
7. Holzmann, F.; Bellino, M.; Siegwart, R.; Bubb, H. Predictive estimation of the road-tire friction coefficient. In Proceedings of the 2006 IEEE Conference on Computer Aided Control System Design, 2006 IEEE International Conference on Control Applications, 2006 IEEE International Symposium on Intelligent Control, Munich, Germany, 4–6 October 2006; pp. 885–890.
8. Sato, Y.; Kobayashi, D.; Kageyama, I.; Watanabe, K.; Kuriyagawa, Y.; Kuriyagawa, Y. Study on Recognition Method for Road Friction Condition. *Trans. Soc. Automot. Eng. Jpn.* **2007**, *38*, 51–56.
9. Yamada, M.; Ueda, K.; Horiba, I.; Tsugawa, S.; Yamamoto, S. Road surface condition detection technique based on image taken by camera attached to vehicle rearview mirror. *Rev. Automot. Eng.* **2005**, *26*, 163–168.
10. Gustafsson, F. Slip-based tire-road friction estimation. *Automatica* **1997**, *33*, 1087–1099.
11. Müller, S.; Uchanski, M.; Hedrick, K. Estimation of the Maximum Tire-Road Friction Coefficient. *J. Dyn. Syst. Meas. Control* **2004**, *125*, 607–617.

12. Yi, K.; Hedrick, K.; Lee, S.-C. Estimation of Tire-Road Friction Using Observer Based Identifiers. *Veh. Syst. Dyn.* **1999**, *31*, 233–261.

13. Li, K.; Misener, J.A.; Hedrick, K. On-Board Road Condition Monitoring System Using Slip-Based Tire-Road Friction Estimation and Wheel Speed Signal Analysis. In Proceedings of the ASME 2006 International Mechanical Engineering Congress and Exposition, Chicago, IL, USA, 5–10 November 2006. https://doi.org/10.1115/IMECE2006-14102.

14. Vahidi, A.; Stefanopoulou, A.; Peng, H. Experiments for Online Estimation of Heavy Vehicle's Mass and Time-Varying Road Grade. In Proceedings of the ASME 2003 International Mechanical Engineering Congress and Exposition. Dynamic Systems and Control, Volumes 1 and 2. Washington, DC, USA, 15–21 November 2003; pp. 451-458.

15. Vahidi, A.; Stefanopoulou, A.; Peng, H. Recursive least squares with forgetting for online estimation of vehicle mass and road grade: Theory and experiments. *Veh. Syst. Dyn.* **2005**, *43*, 31–55.

16. Yong, S.; Li, L.; Yang, C.; Bingjie, Y.; Dongpu, C. A Hybrid Algorithm Combining EKF and RLS in Synchronous Estimation of Road Grade and Vehicle'Mass for a Hybrid Electric Bus. *Mech. Syst. Signal Process*. **2016**, *68–69*, 416-430, ISSN 0888-3270.

17. Raffone, E. Road slope and vehicle mass estimation for light commercial vehicle using linear Kalman filter and RLS with forgetting factor integrated approach. In Proceedings of the 16th International Conference on Information Fusion, Istanbul, Turkey, 9–12 July 2013; pp. 1167–1172.

18. Kiencke, U.; Nielsen, L. Automotive Control Systems: For Engine, Driveline, and Vehicle. Measurement Science and Technology. In *Measurement Science and Technology*; IOP Publishing: Bristol, UK, 2000; Volume 11.

19. Dae, Y.J.; Choi, G. A New Adaptive Mass Estimation Approach of Heavy Truck Based on Engine Torque Local Convex Minimum Characteristic at Low Speeds *Energies* **2020**, *13*, 1649. https://doi.org/10.3390/en13071649.

20. Boada, B.L.; Boada, M.J.L.; Zhang, H. Sensor Fusion Based on a Dual Kalman Filter for Estimation of Road Irregularities and Vehicle Mass Under Static and Dynamic Conditions. *IEEE/ASME Trans. Mechatron.* **2019**, *24*, 1075–1086.

21. *CarSim Database*; Mechanical Simulation Corporation: Ann Arbor, Michigan, USA, 2006.

22. Osborn, R.P.; Shim, T. Independent control of all-wheel-drive torque distribution. *Veh. Syst. Dyn.* **2006**, *44*, 529–546.

23. Doumiati, M.; Charara, A.; Victorino, A.; Lechner, D. *Vehicle Dynamics Estimation using Kalman Filtering: Experimental Validation*; John Wiley & Sons: Hoboken, NJ, USA, 2012.

24. David, E.R.; James, L.M. Learning Internal Representations by Error Propagation. In *Parallel Distributed Processing: Explorations in the Microstructure of Cognition: Foundations*; MIT Press: Cambridge, MA, USA, 1987; pp. 318–362.

25. Kim, P. *MATLAB Deep Learning With Machine Learning, Neural Networks and Artificial Intelligence*; Apress Berkeley: Berkeley, CA, USA, 2017.

26. *CarSim Reference Manual*, version 6.05; Mechanical Simulation Corporation: Ann Arbor, Michigan, USA, 2006.

27. Pacejka, H.B.; Sharp, R.S. Shear Force Development by Pneumatic Tyres in Steady State Conditions: A Review of Modelling Aspects. *Veh. Syst. Dyn.* **1991**, *20*, 121–175.